



# Microencapsulation of Garlic Extract by Complex Coacervation Using Whey Protein Isolate/Chitosan and Gum Arabic/Chitosan as Wall Materials: Influence of Anionic Biopolymers on the Physicochemical and Structural Properties of Microparticles

Loleny Tavares<sup>1</sup> · Hélio Lopes Barbosa Barros<sup>2</sup> · Júlio César Pacheco Vaghetti<sup>2</sup> · Caciano Pelayo Zapata Noreña<sup>1</sup>

Received: 12 September 2019 / Accepted: 7 November 2019 / Published online: 21 November 2019  
© Springer Science+Business Media, LLC, part of Springer Nature 2019

## Abstract

The aim of this study was to encapsulate garlic extract by complex coacervation method using whey protein isolate (WPI)/chitosan (CH) and gum Arabic (GA)/CH as wall materials. Two anionic biopolymers (GA and WPI) were used to find the most suitable wall materials to interact electrostatically with cationic CH. The complex coacervates were freeze-dried to obtain microparticles powders. The microparticles were examined for the nitrogen adsorption/desorption, Fourier transform infrared spectroscopy (FTIR), X-ray diffraction (XRD), thermogravimetric analysis (TGA), differential scanning calorimeter (DSC), sorption isotherms, zeta potential, antioxidant activity, total phenolic content, solubility, moisture content, hygroscopicity, size distribution, and water activity. X-ray diffractograms evidenced microparticles with amorphous structure. WPI/CH and GA/CH microparticles showed surface area of 2.23 and 2.40 m<sup>2</sup> g<sup>-1</sup> and mean pore diameter of 5.20 and 5.37 nm, respectively. The nitrogen adsorption/desorption assay showed that microparticles presented mesopores and macropores that resulted in quick completion of microparticles surface monolayer with nitrogen. The sorption characteristics of microparticles followed the type II isotherm and Guggenheim-Anderson-de Boer (GAB) model was the best model to fit the experimental data. FTIR spectrum of microparticles reveals physical interactions between garlic compounds and functional groups of wall materials, indicating that garlic compounds were intact and encapsulated. TGA results indicated that the wall materials were effective in protecting the garlic sensitive compounds. The negative carboxyl groups (–COO<sup>-</sup>) of GA were better than WPI for coacervation with positive amino groups (NH<sub>3</sub><sup>+</sup>) of chitosan in terms of less hygroscopicity, smaller particle size, and higher retention of garlic phenolic compounds.

**Keywords** Microencapsulation · Garlic extract · Whey protein isolate · Gum Arabic · Chitosan · Complex coacervation

## Introduction

Garlic (*Allium sativum* L.) is widely used around the world as a food and flavoring in cooking. It has been either consumed in raw form or subjected to the processing treatments to obtain secondary products, such as oil, extract, and dried powders

with differences in the content in bioactive compounds (Martins et al. 2016). Garlic extracts have been shown to have strong radical scavenging activity, high activity against plant pathogenic fungi (*Fusarium proliferatum*, *Alternaria brassicicola*, *Magnaporthe grisea*), beneficial effects on arterial stiffness, and endothelial-derived products (Nuutila et al. 2003; Kinalski and Noreña 2014; Peng et al. 2014; Chen et al. 2018; Szulińska et al. 2018). Garlic extracts contain a variety of organosulfur compounds (alliin, allicin, allyl sulfide, (E)-ajoene, (Z)-ajoene, 1,2-vinyldithiin), which allicin represents 70–80% of total thiosulfinate present in garlic (Santhosha et al. 2013; Martins et al. 2016). Organosulfur compounds are responsible for garlic pungent aroma and taste (Amagase et al. 2001). The phenolic, antioxidant, and organosulfur compounds provide garlic therapeutic and biological properties,

✉ Caciano Pelayo Zapata Noreña  
czapatan@ufrgs.br

<sup>1</sup> Institute of Food Science and Technology, Federal University of Rio Grande do Sul, Av. Bento Gonçalves, no. 9500, Porto Alegre, RS 91501-970, Brazil

<sup>2</sup> Institute of Chemistry, Federal University of Rio Grande do Sul, Av. Bento Gonçalves, no. 9500, Porto Alegre, RS 91501-970, Brazil

such as antioxidant, anticancer, antimicrobial, antiinflammatory, hypoglycemic, anticoagulant, cardioprotective, and immunomodulatory activities (Martins et al. 2016). However, the organosulfur compounds of garlic exhibit unpleasant odors, and they are volatile and thermally unstable, losing its biological activity when subjected to high temperatures (Ilić et al. 2017). A variety of encapsulation techniques has been used to protection of garlic bioactive compounds, masking off its flavors and unpleasant odors, such as coacervation (Tavares and Noreña 2019), spray congealing technology (Tomšik et al. 2018), spray drying (Balasubramani et al. 2015), molecular inclusion (Piletti et al. 2019), and liposomes (Pinilla et al. 2017; Pinilla and Brandelli 2016). Complex coacervation is a highly promising microencapsulation technique, employed in various industries, such as the pharmaceutical, food, agriculture, and textile industries (Timilsena et al. 2018). The process involves the spontaneous liquid–liquid phase separation, which occurs through electrostatic interactions between two oppositely charged biopolymers (Bastos et al. 2010). The complex coacervate process is influenced by several factors, such as pH, temperature, ionic strength, molar mass, polymers mixing ratio, total polymers concentration, and charge density (Burgess 1990; Ezhilarasi et al. 2013).

Whey protein isolate (WPI) is an abundant by-product of cheese-making and casein industry. It has been successfully employed in the formation of protein–polysaccharide complexes in the encapsulation process (Eratte et al. 2018).  $\beta$ -Lactoglobulin and  $\alpha$ -lactalbumin are the main components of WPI, being that  $\beta$ -lactoglobulin has well established primary, secondary, tertiary, and quaternary structures, which represent approximately 50% of total whey protein, with isoelectric point of 5.2 (de Souza et al. 2009; Khem et al. 2016). Chitosan is a cationic polysaccharide obtained by alkaline N-deacetylation of chitin. Structurally, it is composed by glucosamine and N-acetylglucosamine units; it is positively charged in acidic environment due to its  $pK_a$  around 6.2–7.0, leading to the protonation of its amino groups in the polymer backbone (Xu et al. 2016; Tavares and Noreña 2019). Chitosan is a natural, biocompatible, biodegradable, nontoxic, and mucoadhesive polymer, which makes it largely used in the different encapsulation process (Peniche et al. 2003; Alishahi and Aider 2012). Gum Arabic is a polysaccharide complex obtained from trunks and branches of two species of acacia trees: *Acacia senegal* and *Acacia seyal* (Shi et al. 2017). Gum Arabic is an anionic polysaccharide ( $pK_a$  of 2.2) and one of the most common wall materials used in microencapsulation process due to its high water solubility, low solution viscosity, good surface activity, and emulsification capacity (Eratte et al. 2014; Tan et al. 2016; Niu et al. 2016).

There are very few reports on encapsulation of garlic extract (Tavares and Noreña 2019; Kinalski and Noreña 2019). In addition, studies about microencapsulation of garlic extract

using complex of whey protein isolate/chitosan and gum Arabic/chitosan followed by freeze-drying process have not yet been performed. The objectives of this study were characterize the obtained freeze-dried coacervates through several forms of analyses, including nitrogen adsorption/desorption, FTIR, TGA, X-ray diffraction, sorption isotherms, zeta potential, antioxidant activity, total phenolic content, solubility, moisture content, hygroscopicity, size distribution, and water activity.

## Materials and Methods

### Materials

Garlic bulbs were acquired from a local market in Porto Alegre, Brazil. Chitosan (CH) samples with the degree of deacetylation of 96% and whey protein isolate (WPI) were kindly donated by Primex (Siglufjordur, Iceland) and Arla Foods Ingredients (São Paulo, Brazil), respectively. Gum Arabic (Instantgum BA) was purchased from Nexira (São Paulo, Brazil). Glacial acetic acid and sodium acetate trihydrate were purchased from CAQ-Casa da Química (Diadema, Brazil). Sodium hydroxide (NaOH), hydrochloric acid (HCl), and acetic acid both with analytical grade were purchased from Sigma-Aldrich.

### Preparation of Garlic Extract

The garlic extract was prepared according to Tavares and Noreña (2019) with minor modifications. Garlic bulbs were crushed and mixed at a ratio of 1:2 (w/v) with two different solutions of acetate buffer (100 mM) previously prepared at pH 5.5 and 3.6. The mixture was sonicated in an ultrasonic bath (Elmasonic S 30 ultrasonic bath) at 37 kHz and then centrifuged (Thermo Fisher Scientific, Heraeus Megafuge 16R) at 10,000 $\times g$  for 10 min at 4 °C. The resultant supernatant was collected, passed through 0.22- $\mu m$  membranes (Millipore, Billerica), and stored in sterilized glass containers in the absence of light at  $-20$  °C for subsequent processing.

### Microencapsulation Process

#### Complex Coacervation Systems

The garlic extract (GE) was encapsulated using complexes of WPI/CH and GA/CH as wall materials. The WPI 3% (w/w) and GA 3% (w/w) dispersions were prepared in acetate buffer (100 mM) at pH 6 and 3.6, respectively. CH 3% (w/w) dispersions were prepared by dispersing CH powders in solutions of garlic extract previously prepared at pH 5.5 and 3.6, resulting in two dispersions of CH 3% (w/w). For WPI/CH, the optimum conditions for their coacervation were pH 5.8

and WPI to CH ratio of 5:1 (w/w) (Tavares and Noreña 2019). For GA/CH, the pH was 3.6 and GA to CH ratio of 5:1 (w/w) (Butstraen and Salaün 2014). Subsequently, the CH 3% (w/w) dispersions prepared at pH 5.5 and 3.6 were mixed with WPI 3% (w/w) and GA 3% (w/w), respectively. The final pH of both complexes was adjusted using 0.1 M HCl. Then, the dispersions were agitated in a mechanical stirrer at 200 rpm for 20 min. Afterward, the dispersions were allowed to rest for 5 h. Thereafter, two phases were formed: a solvent-rich phase (supernatant) and a solvent-depleted liquid (precipitated coacervate). The supernatants were discarded, and each precipitated coacervate was collected and frozen in ultra-freezer (Liobras, Liotop UFR 30) at  $-68\text{ }^{\circ}\text{C}$  for 24 h. The frozen coacervates were dried in a freeze-dryer (Liobras, LIOTOP L101) at  $-57\text{ }^{\circ}\text{C}$  at vacuum pressure less than 6.65 Pa for 48 h. Then, the samples were crushed using a mortar and pestle. The resultant microparticles were placed in polyethylene bags, sealed, and placed in aluminum pouches. The samples were stored in a desiccator containing silica for further analyses.

## Freeze-Dried Powder Characterization

### Solubility, Moisture Content, Hygroscopicity, and Water Activity

The solubility of powders was determined as previously described by Cano-Chauca et al. (2005). One gram of powder was added to 100 mL of distilled water under stirring condition with a magnetic stirrer. The resultant dispersion was centrifuged at  $3000\times g$  for 5 min. Then, a 25-mL aliquot of the supernatant was transferred to previously weighed Becker and incubated at  $105\text{ }^{\circ}\text{C}$  for 24 h. The solubility (%) was calculated by the weight difference.

The moisture content was determined gravimetrically by drying in an oven at  $105\text{ }^{\circ}\text{C}$  until constant weight, according to AOAC (1990).

Hygroscopicity was determined according to Cai and Corke (2000) with minor modifications. One gram of spray-dried powder sample was placed in a container with a saturated NaCl solution (75% RH) and stored in an incubator chamber (411/FDP Ethik Technology) at  $25\text{ }^{\circ}\text{C}$  for 1 week. Then, the weight of samples was registered until equilibrium was reached. Hygroscopicity was expressed as gram of adsorbed moisture per 100 g of dry basis.

Water activity ( $a_w$ ) was measured using a water activity meter (AquaLab 3TE-Decagon, Pullman, USA) at  $25\text{ }^{\circ}\text{C}$ .

### Zeta Potential Analysis

The zeta potential of powders was determined using a ZetaPALS (Brookhaven Instruments, 31450) equipment. For the measurement, 0.5 g of powder was diluted with 50 mL of

distilled water and kept under magnetic stirring for 1 min. Then, the samples were placed into a  $\zeta$ -potential cell and measurements were carried out in duplicate at  $20\text{ }^{\circ}\text{C}$ .

### Particle Size Distribution and Span Value

Particle size distribution of powders samples was performed using a laser granulometer (CILAS, 1180), and the analysis was carried out in the range of 0.04–2500  $\mu\text{m}/100$  classes. The samples were dispersed in isopropanol, under constant magnetic stirrer and then sonicated for 60 s. The particle size was expressed as volume mean diameter ( $D_{[4,3]}$ ). The span value (SPA) was calculated with the following equation:  $\text{SPA} = (D_{90} - D_{10})/D_{50}$ , where  $D_{90}$ ,  $D_{10}$ , and  $D_{50}$  are the volume diameters at 90%, 10% and 50% of the cumulative size, respectively.

### Morphology

The morphology of microparticle powders was observed with a scanning electron microscope (Carl Zeiss, EVO, MA10) equipment operating at 10 kV and magnification of  $\times 300$ . Previously, the powders were attached to double-sided adhesive carbon tape fixed to aluminum stubs and metallized with a thin layer of gold.

### Nitrogen Adsorption and Desorption Isotherms

The nitrogen adsorption–desorption isotherms were obtained using a Tristar II 3020 (Micromeritics Instrument Corporation) equipment at the temperature of 77 K (the liquid nitrogen boiling point). For characterization of microparticles, the specific surface areas were determined from the BET method (Brunauer et al. 1938); the average pore diameter was calculated by BET method. The pore size distribution curves were obtained using BJH (Barrett et al. 1951) method. The BJH was used to determine the adsorption and desorption cumulative surface area of pores from the range between  $17\text{ \AA} < \text{diameter} < 3000\text{ \AA}$  and the BJH adsorption and desorption cumulative volume of pores between  $17\text{ \AA} < \text{diameter} < 3000\text{ \AA}$ .

### Moisture Sorption Isotherms

The equilibrium moisture contents of the powder samples were determined by the static gravimetric method recommended by the COST 90 Project (Spiess and Wolf 1983). Nine saturated saline solutions (lithium chloride, potassium acetate, magnesium chloride, potassium carbonate, sodium nitrite, sodium chloride, potassium chloride, barium chloride, and copper sulfate) were used to obtain relative humidity ranging from 11 to 98% (Young 1967). One gram of each sample was placed into beaker and then stored in small glass desiccators with clamp lids, each containing respective

saturated salts solutions with different relative humidities. A beaker containing toluene was also placed into jars to prevent microbial spoilage (Lago and Noreña 2015). The small glass desiccators were placed in an air-circulating, hermetically insulated, temperature-controlled equipment (BOD TE 381 Tecnal, Piracicaba, SP, Brazil) maintained at 25 °C until equilibrium was reached (3 weeks). Then, the moisture content was determined gravimetrically by drying in an oven at 105 °C until constant weight. The models used to fit the experimental sorption data are shown in Table 2. The parameters of these equations were determined using MATLAB curve fitting tool® (Mathworks, MA, USA, version R2016b).

The coefficient determination ( $R^2$ ) and the mean relative percentage deviation modulus ( $E$ ) were used to determine the goodness of fit of the models. The  $E$  was calculated according to Eq. 1:

$$E (\%) = \frac{100}{N} \sum_{i=1}^N \frac{|X_{ei} - X_{pi}|}{X_{ei}} \quad (1)$$

where  $X_{ei}$  and  $X_{pi}$  are the measured and predicted equilibrium moisture content and  $N$  is the number of observations.

### X-Ray Diffraction

The X-ray diffractograms of powders were obtained from the X-ray diffractometer (Siemens D5000, Bruker) equipment using Cu-K $\alpha$  radiation with a wavelength of 1.5406 Å at 40 kV and 25 mA. The diffraction data were collected at  $2\theta$  angle range from 3 to 80°.

### Fourier Transform Infrared Spectroscopy

The FTIR spectra of microparticles, wall materials, and garlic powder, obtained through garlic aqueous extract, were characterized by a FTIR Spectrophotometer (Shimadzu 8400, Japan) using potassium bromide (KBr) pellets. All spectra were taken in the range of 4000 to 400  $\text{cm}^{-1}$  with a resolution of 4  $\text{cm}^{-1}$ .

### Thermal Analysis

Thermogravimetric analyses of WPI/CH and GA/CH microparticles powders were performed on a TA Instruments (SDT Q600) thermogravimetric analyzer. Approximately 10 mg of samples was placed on the platinum pan and kept under a nitrogen atmosphere with a flow rate of 50  $\text{mL min}^{-1}$  and heated in the temperature range of 20 to 800 °C, at heating rate of 10 °C  $\text{min}^{-1}$ .

### Total Polyphenols Content and Antioxidant Capacity

Before the analysis, the coating material structure of the powders was completely destructed as previously described by Robert et al. (2010) with some modifications. One gram of powder was suspended in 10 mL of solution formed by a mixture of acetonitrile with methanol:acetic acid:water (50:8:42, v/v/v) at a ratio of 1:1 (v/v). The dispersions were sonicated at 37 kHz for 2 min and then centrifuged at 10,000 $\times g$  for 10 min at 4 °C. The resultant supernatant was collected, passed through 0.22- $\mu\text{m}$  membranes, and stored in sterilized glass containers until the analysis.

The total phenolic content (TPC) of the microparticles and garlic extract, obtained at pH 5.5 and 3.6, were determined as described by Singleton and Rossi (1965). The spectrophotometric absorbance was measured at 765 nm in a UV–Vis spectrophotometer (Thermo Scientific, Genesys 10S). The TPC in powders and garlic extract was estimated as gallic acid equivalents (GAE) per gram of sample on a dry basis (d.b.).

The TPC retention efficiency was evaluated considering the ratio between total phenolic content present in freeze-dried powders and in garlic extract before drying.

The antioxidant activity was determined by ABTS assay as reported by Re et al. (1999). The absorbance was measured in a spectrophotometer at 734 nm. The antioxidant activity of the powders and garlic extract was reported as micromoles of Trolox equivalent (TE) per gram of sample on a dry basis (d.b.).

### Statistical Analysis

Statistical analysis was performed using SAS software (v. 9.3). Data were subjected to analysis of variance (ANOVA), and mean comparison of different treatments was carried out using Tukey's test ( $p < 0.05$ ).

## Results and Discussions

### Potential Zeta

Potential zeta value is a key indicator of surface charge of microparticles and provides important information about their stability against coalescence and aggregation in dispersions (Choi and Chang 2018). WPI/CH and GA/CH microparticle powders were dispersed in distilled water and the pH of dispersion was 3.70 and 5.75, respectively. Therefore, the CH present in both dispersions was predominantly positively charged ( $\text{p}K_a$  around 6.3), WPI was predominantly negatively charged (isoelectric point,  $\text{pI}$ , around 5.2), and GA negatively charged ( $\text{p}K_a$  of 2.2) (de Souza et al. 2009; Lam et al. 2018; Eratte et al. 2014; Tan et al. 2016).

The Zeta potential values of the WPI/CH and GA/CH microparticles were  $15.25 \pm 0.85$  and  $16.01 \pm 2.21$  mV,



respectively. These results indicate that microparticles present a positive surface charge when they are dispersed in water. The freeze-dried coacervates resulted mainly due to electrostatic interactions between the positive amino groups ( $\text{NH}_3^+$ ) of CH and negative carboxyl groups ( $-\text{COO}^-$ ) of GA and WPI. The amount of CH used to encapsulate was 5 times less than the gum Arabic and WPI. However, the positive surface charge showed that CH had a significant contribution in the zeta potential values. The  $\zeta$ -potential values higher than 30 mV or less than  $-30$  mV indicates a stable dispersion due to electrostatic repulsion (Cabuk et al. 2016). In this sense, the dispersions of microparticle powders in the distilled water resulted in an unstable system with the occurrence of microparticles coalescence and aggregation. These results were to be expected once the coacervates formed through electrostatic interactions, where the dispersion becomes electrically unstable, with the charge closer to zero (Rocha-Selmi et al. 2013).

### Physical Properties of Powders

The moisture content and water activity are important variables for the shelf life of the microparticles. The WPI/CH and GA/CH presented very low moisture content with values of 3.77% and 2.06% (d.b.), respectively (Table 1). The moisture content of the WPI/CH powders was similar to those found in the encapsulation of the garlic extract by spray drying process (Tavares and Noreña 2019). In both drying processes, the powders present moisture content in the range between 3 and 10%, which means a good stability during storage (Quispe-Condori et al. 2011). Both powders presented low moisture content and water activity values below to 0.2 (Table 1), which promote lower hydrolytic reactions, enzyme activity, and free or minimum growth rates of microorganisms, such as molds, yeasts, and bacteria during storage (Damodaran and Parkin 2017). The powders showed low solubility in water, as results of employed complex coacervation technique, where the formation of water insoluble complex occurs (Rocha-Selmi et al. 2013). However, the microparticles can be used as ingredients and applied into solid, semisolids, and liquid food products.

The hygroscopicity was 18.88 and 14.87% for WPI/CH and GA/CH, respectively (Table 1). The high hygroscopicity of the powders is related to the high number of hydrophilic groups present in the structure of microparticles available to adsorb water molecules from the ambient air (Tonon et al.

2009). In addition, the powders presented lower moisture content, which means that they have a greater capacity to adsorb moisture from the ambient air (Tonon et al. 2008). The microparticles showed high hygroscopicity, which making necessary its careful handling and using of high-barrier packaging materials during the storage in humid environments (Tavares and Noreña 2019).

### Particle Size Distribution and Morphology of the Powders

The granulometric analysis allows to evaluate the particle size distribution of materials. The powder particle size distribution is shown in Fig. 1. The microcapsules exhibited a unimodal distribution with higher values of  $D_{[4,3]}$  for WPI/CH microparticles. The values of average diameter,  $D_{10}$ ,  $D_{50}$ , and  $D_{90}$  determined by laser diffraction and calculated span values are shown in Table 1. The value of  $D_{[4,3]}$ , is related to the mean diameter, in volume, corresponding to the diameter of the spherical particles with the same mean volume of the system particles (da Costa et al. 2015). Analyzing the results of Table 1, it showed that 90%, 50%, and 10% of WPI/CH microparticles samples were smaller than 293.52, 103.39, and 25.06  $\mu\text{m}$  and for GA/CH microparticles, the values were 189.21, 74.23, and 19.18  $\mu\text{m}$ , respectively. The process parameters used to obtain microparticles and its components affect the particle size, such as the type of core material, concentrations of wall materials, the stirring speed, and polymer molecular weight (Krishnamachari et al. 2007). In addition, both microparticles presented high size as result of freeze-drying process and the manually process using a mortar and pestle in the end of drying to obtain powders (Kuck and Noreña 2016; Chen Chen et al. 2012). The span values were greater than 1 (Table 1) that indicates a wide distribution of particle sizes (Noreña et al. 2015).

SEM images of the WPI/CH and GA/CH microparticles are shown in Fig. 2. Both microparticles showed irregular shapes of varying sizes and resembled broken glass or flake-like structure, characteristic of powders obtained by the freeze-drying process. The microparticles also exhibited smooth surface without cracks fissures and pores on the nanometric scale (1–100 nm), as reported in (Table 2). Therefore, it is not perceptible in the SEM images at magnification of  $\times 300$ . SEM images show larger particle sizes for WPI/CH than for GA/CH, collaborating with the results obtained in the particle size distribution

**Table 1** Physical–chemical properties of WPI/CH and GA/CH microparticles obtained by complex coacervation followed by freeze-drying process

Powder	Solubility (%)	Water activity	Moisture content (%)	Hygroscopicity (%)	$D_{10}$ ( $\mu\text{m}$ )	$D_{50}$ ( $\mu\text{m}$ )	$D_{90}$ ( $\mu\text{m}$ )	Span
WPI/CH	$39.49 \pm 3.96^a$	$0.108 \pm 0.002^a$	$3.73 \pm 0.32^a$	$18.88 \pm 1.86^a$	$25.06 \pm 1.65^a$	$103.39 \pm 1.49^a$	$293.51 \pm 20.70^a$	$2.60 \pm 0.14^a$
GA/CH	$34.39 \pm 3.16^a$	$0.054 \pm 0.003^b$	$2.06 \pm 0.28^b$	$14.87 \pm 0.19^b$	$19.18 \pm 0.46^b$	$74.23 \pm 1.17^b$	$189.21 \pm 4.35^b$	$2.29 \pm 0.03^b$

Values (mean  $\pm$  SD) in a column with different letters are significantly different ( $p < 0.05$ ) based on Tukey's multiple comparison test

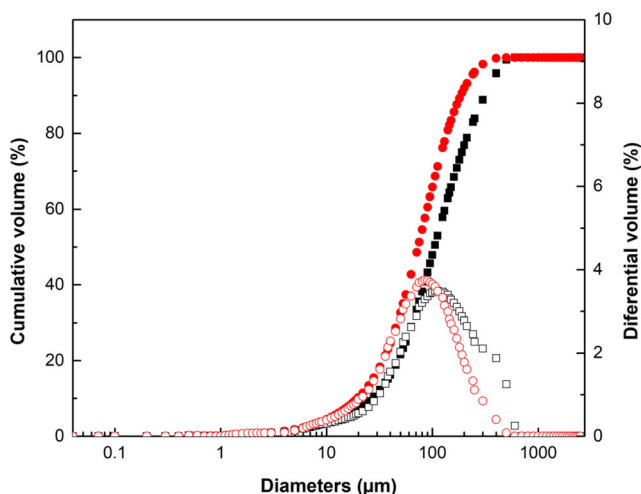


**Fig. 1** Particle size distributions of GA/CH (circle) and WPI/CH (square) microparticles. The cumulative volume (%) and differential volume are represented by close and open symbols, respectively

analysis. Similar microparticle morphology has been reported for freeze-dried powder as consequence of freeze-drying process (Chen et al. 2012).

### Nitrogen Adsorption and Desorption Isotherms

Nitrogen adsorption and desorption isotherms at 77 K for WPI/CH and GA/CH powders are shown in Fig. 3a. The adsorption–desorption isotherms of both powders belong to type II, with not a clear evidence on the transition point from monolayer to multilayer nitrogen gas adsorption, suggesting a rapid completion of monolayer coverage (Sing 1985). The course of the isotherm for both microparticles is characterized by stronger adsorption of nitrogen (Włodarczyk-Stasiak et al. 2014). The hysteresis loops verified can be classified as type H3, which is usually associated with slit-shaped pores and powders with abundant pore structure (Liu et al. 2015; Fu et al. 2010). The pore size distributions are represented in Fig. 3b, revealing similar curve behavior of WPI/CH and GA/CH microparticles. It is also verified absence of the characteristic peak on the pore distribution curve may demonstrate an irregularity in the microparticles structure (Włodarczyk-

Stasiak et al. 2014). IUPAC classified pores into the following groups: macropores > 50 nm, mesopores in the range of 2.0 to 50 nm, and micropores < 2.0 nm (Sing 1985). In this sense, the distribution of average pore diameter curve indicated a predominance of mesopore and macropore structure in the powders.

The surface area, average pore size diameter, and pore volume of the microparticles measurements at 77 K are presented in Table 2. The microparticles exhibited similar surface area and pore diameters, which are in accordance with the results reported in Fig. 3a for nitrogen adsorption/desorption isotherms and the pore size distribution curves represented in Fig. 3b. The powders showed very smallest pores on the surface, which is desirable in order to increase its storage stability (Premi and Sharma 2017).

### Moisture Sorption Isotherms

Sorption isotherm provides important information about how WPI/CH and GA/CH microparticles will behave when subjected to different relative air humidity (Fig. 4). The estimated parameters for all the sorption models are shown in Table 3. The GAB and Oswin models provided the best fit to the experimental data, when considering the lowest value of the average relative deviation ( $E$ ) for both microparticles. According to the results of  $E$  values above 10%, the other models failed to describe the sorption isotherms of experimental dates (Lomauro et al. 1985). The GAB model was chosen to describe the isotherms behavior, since it is largely used in literature and recommended by the European Group Cost 90 for the investigation of physical characteristics in food products (Wolf et al. 1985). Regarding to the GAB parameters, the moisture content of the monolayer ( $X_m$ ) is related to the physical and chemical stability of foods, influencing the lipid oxidation, enzyme activity, nonenzymatic browning, flavor preservation, and product structure (Koç et al. 2010). The  $X_m$  value was lower for GA/CH than WPI/CH microparticles, which represent lower adsorption of water molecules in the microparticles monolayer (Santos et al. 2015). These results suggested its higher physical and chemical stability, which is also

**Fig. 2** Scanning electron microscopy images of garlic extract microencapsulated from complex coacervate of **a** whey protein isolate (WPI)/chitosan (CH) and **b** gum Arabic (GA)/chitosan (CH) obtained by freeze-drying process at magnification of  $\times 300$

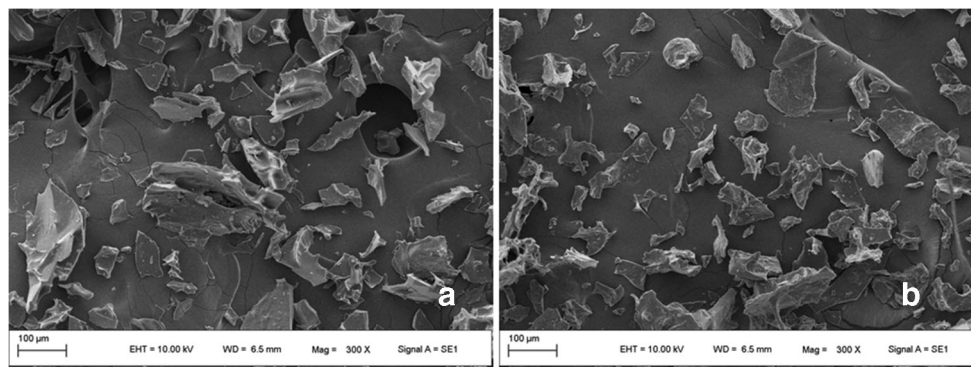


**Table 2** Surface area and porosity of WPI/CH and GA/CH microparticles obtained by complex coacervation followed by freeze-drying process

Powder	BET surface area ( $\text{m}^2 \text{g}^{-1}$ )	Average pore diameter by BET (nm)	BJH adsorption cumulative surface area of pores ( $\text{m}^2 \text{g}^{-1}$ )	BJH desorption cumulative surface area of pores ( $\text{m}^2 \text{g}^{-1}$ )	BJH adsorption cumulative volume of pores ( $\text{cm}^3 \text{g}^{-1}$ )	BJH desorption cumulative volume of pores ( $\text{cm}^3 \text{g}^{-1}$ )
WPI/CH	2.23	5.20	1.54	1.80	0.0025	0.0022
GA/CH	2.40	5.37	1.73	1.97	0.0027	0.0025

related with its lower moisture content, water activity and hygroscopicity (Table 1). The values of constants  $k$  and  $C$  are in the range of  $0.24 < k \leq 1$  and  $5.67 \leq C \leq \infty$ , respectively, which represent the limit values that describes well sigmoidal type II isotherms (Lewicki 1997). The parameter  $k$  reflecting properties of multilayer molecules with respect to the bulk liquid and the Guggenheim constant  $C$  is related to the monolayer heat of sorption and allow quantifying the energy difference between adsorption in the form of one monolayer and/or in several multilayers (Almeida et al. 2018; Anderson 1946). For both samples, the values of  $k < 1$ , indicating that the water molecules present in the monolayer were more strongly bound than those in the multilayer (Arthur et al. 2018). The constant  $C$  was higher in GA/CH microparticles, revealing stronger bonds between water molecules and the hydrophilic sites at the monolayer of the microparticles (Almeida et al. 2018).

The isotherms obtained according to GAB Model (Fig. 4) showed the typical sigmoid shape of type II isotherm, according to the BET classification (Brunauer et al. 1940). In both powders, the equilibrium moisture content ( $X_e$ ) increased with the increase of water activity ( $a_w$ ). The microparticles showed higher capacity to adsorb water at high water activities. These results are mainly due to the high hygroscopic capacity of the microparticles, resulting in powders with a great capacity to adsorb larger quantities of water at high relative humidity conditions. Due to absence of previous study of microencapsulation and sorption isotherms using WPI/CH and GA/CH complex coacervates, this made it difficult to compare our results.

## X-Ray Diffraction

The X-ray diffraction (XRD) analysis was performed to confirm the crystalline or amorphous nature of dried microparticles powders. Powders with crystalline state present well-ordered regions with a series of sharp and defined peaks, while amorphous products produce a broad peak due to its disordered state (Kang et al. 2019). The X-ray diffraction spectra of the powders are shown in Fig. 5. For individual wall materials, GA exhibited one broad peak at  $2\theta$  of  $20^\circ$ , demonstrating an amorphous structure. WPI showed two broad peaks at  $2\theta$  of  $8.5^\circ$  and  $19.6^\circ$ , revealing an amorphous structure with minimum crystallinity. CH exhibited two sharp and defined peaks at  $2\theta$  of  $10^\circ$  and  $20^\circ$ , which exhibited a more ordered structure and a clearly higher crystallinity when compared with GA and WPI. These results are in agreement with XRD that are reported for CH (Hosseini et al. 2013), GA (Kang et al. 2019), and WPI (Fernandes et al. 2014).

GA/CH and WPI/CH microparticles revealed amorphous structure with characteristics broader peaks. The diffractogram of GA/CH powder presented one broader peak pattern at  $2\theta$  of  $10^\circ$ . This result suggests that the crystalline structure of CH was disrupted by electrostatic interactions between GA and CH, resulting in microparticles with amorphous structure. Tan et al. (2016) also used complex of GA/CH in the encapsulation of curcumin, which resulted in powders with an amorphous state after CH interacting with oppositely charged GA (2016). Similar results were verified in

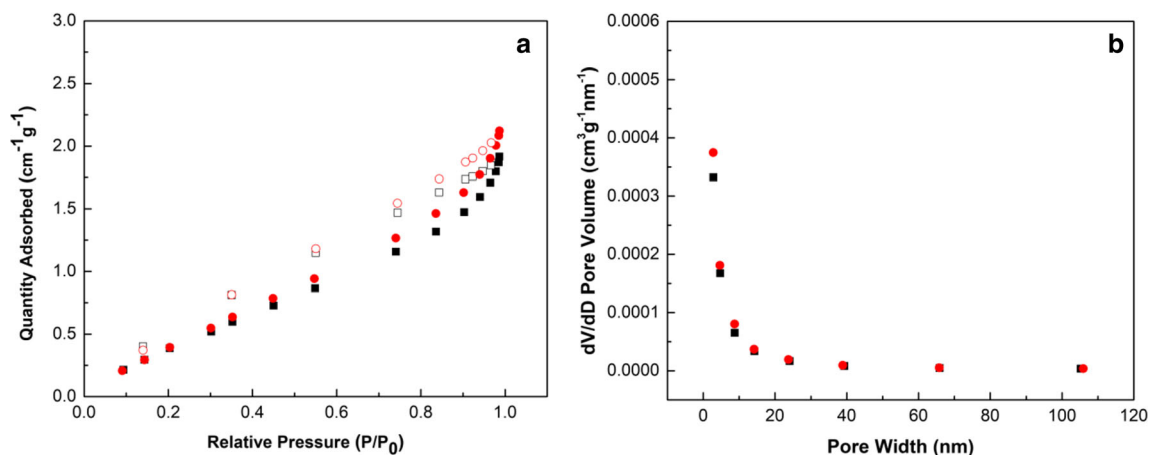


**Fig. 3** Analyses of nitrogen adsorption (close symbols) and desorption (open symbols) isotherms obtained at 77 K (a) and pore size distribution (b) for the WPI/CH (square) and GA/CH (circle) microparticles

**Fig. 4** Sorption isotherms of the WPI/CH and GA/CH microparticles at 25 °C adjusted to the GAB model, representing by WPI/CH (GAB) and GA/CH (GAB), respectively

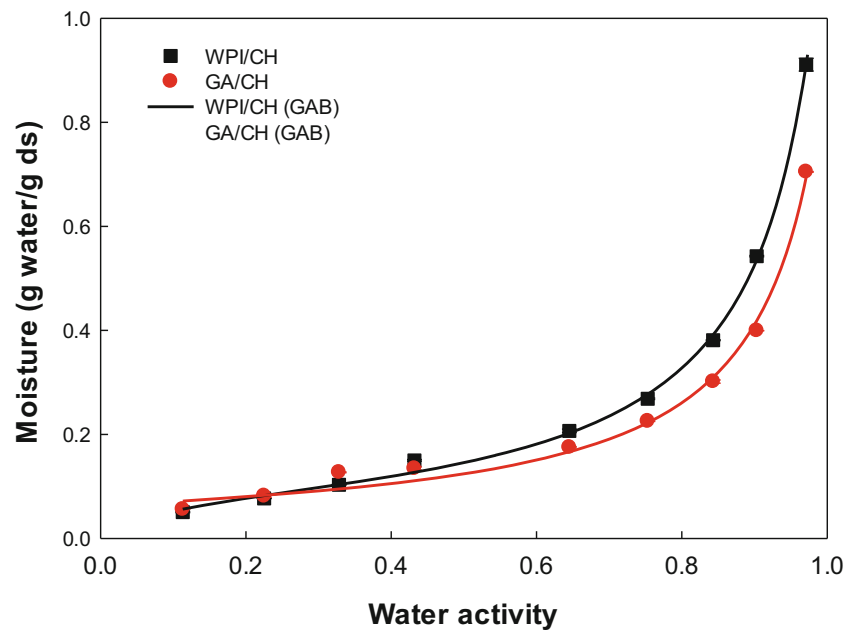


**Table 3** Estimated parameters of the isotherm models for WPI/CH and GA/CH microparticles obtained by complex coacervation followed by freeze-drying process

Model	Equation	Constant	WPI/CH	GA/CH
GAB	$X = \frac{C \cdot K \cdot X_m \cdot a_w}{(1 - K \cdot a_w) \times (1 - K \cdot a_w + C \cdot K \cdot a_w)}$	$X_m$	0.085	0.067
		$C$	12.46	222
		$k$	0.935	0.931
		$R^2$	0.998	0.993
		$E$	4.797	9.721
Halsey	$X = \left( \frac{-A}{\ln a_w} \right)^{\frac{1}{B}}$	$A$	0.027	0.015
		$B$	1.841	1.981
		$R^2$	0.986	0.994
		$E$	20.426	10.149
Henderson	$X = \left[ \frac{\ln(1 - a_w)}{-A} \right]^{\frac{1}{B}}$	$A$	3.905	5.202
		$B$	0.852	0.954
		$R^2$	0.986	0.957
		$E$	22.698	25.635
Smith	$X = A + (B \times \log(1 - a_w))$	$A$	-0.011	0.020
		$B$	-0.243	-0.177
		$R^2$	0.976	0.961
Oswin	$X = A \cdot \left[ \frac{a_w}{1 - a_w} \right]^B$	$E$	21.523	17.096
		$A$	0.165	0.1433
		$B$	0.491	0.453
		$R^2$	0.994	0.997
		$E$	8.587	4.574

$X$  is equilibrium moisture content (g water  $g^{-1}$  d.b.) and  $a_w$  is water activity;  $X_m$  is the monolayer moisture content (g water  $g^{-1}$  d.b.) and  $a_w$  is water activity; and  $A$ ,  $B$ ,  $C$ , and  $k$  are parameters of each model.  $R^2$  is the coefficient of determination, and  $E$  is the mean relative percentage deviation modulus



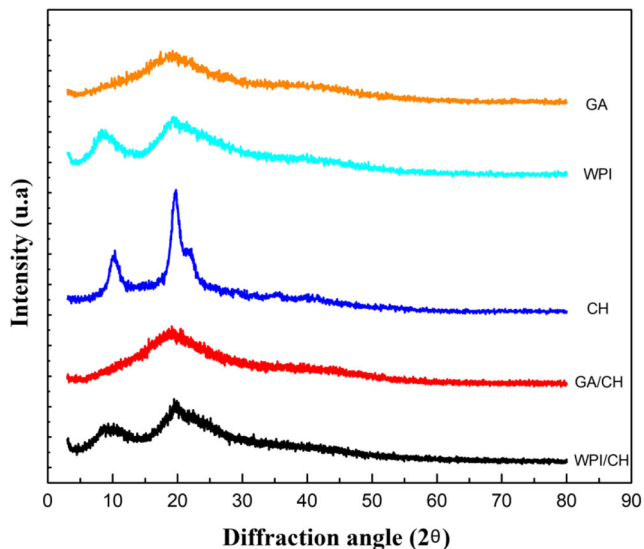


**Fig. 5** X-ray diffractogram of individual wall materials (GA, CH, and WPI) and microparticles (GA/CH and WPI/CH)

diffractogram of WPI/CH microparticles, which presented two broader peak patterns with low and high intensities at  $2\theta$  of  $10^\circ$  and  $19.8^\circ$ , respectively. These results suggest the electrostatic interactions between WPI and CH, which resulted in microparticles powders with an amorphous structure with similar characteristics of WPI diffraction spectrum. According to Borrmann et al., powders with amorphous structure tend to have high hygroscopicity due to high water adsorptions from the relatively moist environment during storage (Borrmann et al. 2013), confirming the obtained results of high hygroscopicity (Table 1).

### Fourier Transform Infrared Spectroscopy

The infrared spectra of the wall materials (GA, CH and WPI), microparticles, and freeze-dried garlic extract are shown in Fig. 6. For wall materials (Fig. 6a), the chitosan powder showed characteristic peaks at  $3400\text{ cm}^{-1}$  (OH and  $\text{NH}_2$  stretching),  $2954\text{ cm}^{-1}$  (CH stretching),  $1654\text{ cm}^{-1}$  (attributed to C=O vibration of the acetylated units ( $-\text{CONH}_2$  groups, amide I)),  $1410\text{ cm}^{-1}$  (vibration of  $-\text{OH}$  and  $-\text{CH}$ ), and  $1085\text{ cm}^{-1}$  (C–O–C stretching). The WPI showed peaks at  $1417\text{ cm}^{-1}$  (N–H bending and C–N stretching vibrations, amide III),  $1544\text{ cm}^{-1}$  (amide II),  $1654\text{ cm}^{-1}$  (C=O stretching vibrations and amide I),  $2954\text{ cm}^{-1}$  (C–H stretching), and  $3340\text{ cm}^{-1}$  (O–H and N–H stretching vibrations). GA showed a typical band at  $3400\text{ cm}^{-1}$  (O–H stretching),  $2922\text{ cm}^{-1}$  (C–H stretching),  $1641\text{ cm}^{-1}$  (C=O stretching),  $1400\text{ cm}^{-1}$  (C–H bending), and  $1085\text{ cm}^{-1}$  (C–O stretching). The set of bands presented in this study was reported in our other study and also by other authors, such as for chitosan (Huang et al. 2012; Tavares and Noreña 2019), whey protein isolate (González-Martínez

et al. 2017; Tavares and Noreña 2019), and gum Arabic (Espinosa-Andrews et al. 2010).

For microparticles (Fig. 6b), the WPI/CH and GA/CH showed characteristics broad band at  $3400\text{ cm}^{-1}$  concerned with OH groups of individual biopolymers and overlapped the stretching band of NH. In addition, the microparticles showed bands characteristics of individual biopolymers used in the formation of complex coacervate, confirming the presence of both individual biopolymers in the freeze-dried coacervate. However, the FTIR of freeze-dried coacervates is not conclusive in relation to the formation of electrostatic interaction between biopolymers, since the bands of microparticles do not change significantly in the carbonyl-amide region (Espinosa-Andrews et al. 2010). These results are mainly due to the presence of compounds present in garlic extract,

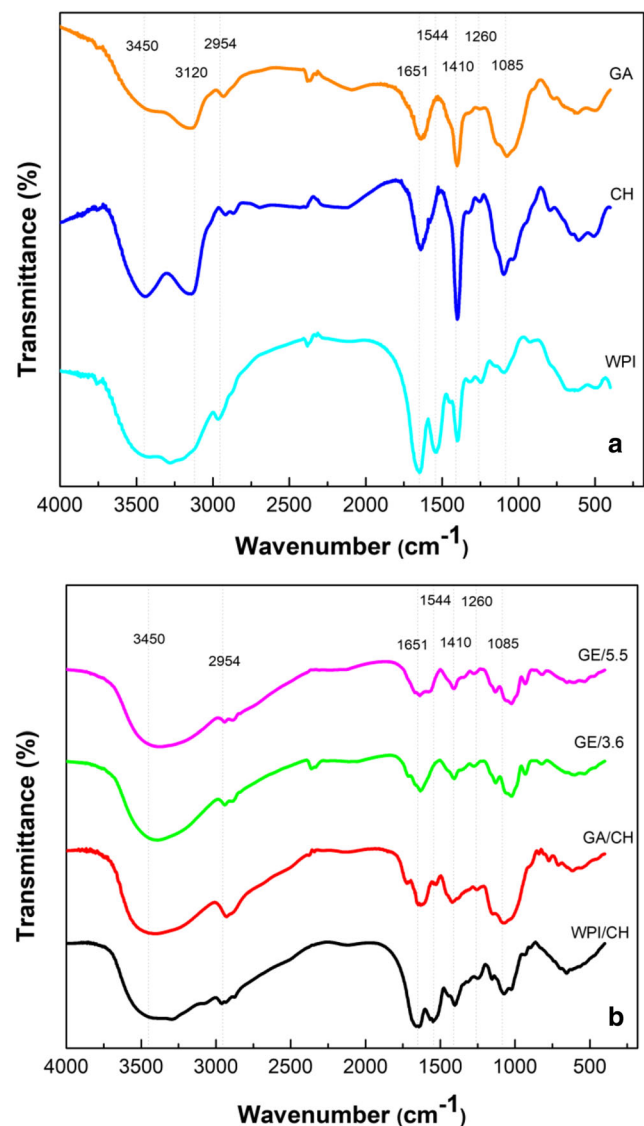


**Fig. 6** FTIR spectra of individual wall materials (GA, CH, and WPI) microparticles (a) and powders of GA/CH, WPI/CH, and lyophilized garlic extract prepared at pH 5.5 (GE/5.5) and pH 3.6 (GE/3.6) (b)

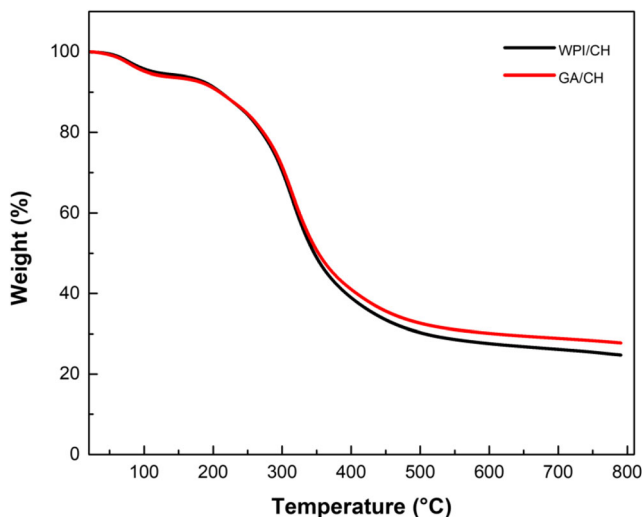


**Fig. 7** The thermogravimetric analysis (TGA) curve of GA/CH and WPI/CH microparticle powders

which have similar functional groups of wall materials and their bands appears at the same value of wavenumber. The FTIR spectrum of freeze-dried garlic extract prepared at pH 3.6 (GE/3.6) and pH 5.5 (GE/5.5) showed peaks on the same wavenumber, which means the presence of same chemical groups of the components present in garlic extract. Pinilla et al. reported similar FTIR spectrum of garlic extracted with distilled water (2017). Both freeze-dried garlic extract and microparticles revealed similar band profiles with the same wavenumber, indicating the presence of intact garlic compounds in the complex coacervates and effectiveness of the process of encapsulation. In addition, the absence of new peak on the FTIR spectrum of microparticles suggests not chemical reaction between compounds present in garlic extract and functional groups of wall materials. These results suggest a predominance of physical interactions in the encapsulation process (Meng et al. 2017; Tavares and Noreña 2019).

### Thermogravimetric Analysis

The thermogravimetric analysis (TGA) of the GA/CH and WPI/CH microparticles is given in Fig. 7. Both microparticles showed three thermal events of mass loss. The first event in the range of 20 and 105 °C, with weight loss about 4%, is

attributed to the evaporation of adsorbed water on the microparticles surface and unencapsulated volatile compounds present in garlic extract. The second event from 150 and 400 °C, with weight loss about 62%, is attributed to the decompositions and depolymerization of wall materials constituents, such as the cleavage of S–S, O–N, and O–O linkages and consequently the breakdown of covalent peptide bonds in WPI (Azizi et al. 2018); the depolymerization and degradation of chitosan D-glucosamine and N-acetyl-D-glucosamine units (Gámiz-González et al. 2017); and carbohydrate ring dehydration, decomposition, and depolymerization for GA (Fernandes et al. 2016). This event also causes evaporation and decompositions of garlic compounds that became unprotected. During the third step, up to 450, the weight loss continued but it was less accentuated with decomposition of residual microparticles compounds. Both microparticles samples are thermally stable up to 220 °C, representing the maximum temperature where the wall materials effectively protect the heat sensitive compounds present in garlic extract (organosulfur compounds). The high thermal stability of microparticles is desired property, since the microparticles could be used as ingredients in the elaboration of thermally processed food.

### Total Phenolic Content and Antioxidant Activity

The total phenolic content (TPC) and antioxidant activity of the GE (pH 3.6 and 5.5) and microencapsulated powders are shown in Table 4. The garlic phenolic compounds extracted at pH 3.6 was significantly ( $p < 0.05$ ) higher than shown in GE extracted at pH 5.5, revealing its more stability at more acid pH, since the extractions were conducted under the same process conditions. Similar results of TPC present in GE (d.b.) was reported by Lu et al. with TPC ranging from 15.75 to 19 mg gallic acid  $g^{-1}$  (fresh weight) (2011). The difference in garlic TFC is expected since the garlic phenolic content depends on the genetic factors, cultivation conditions, weather conditions, plant location, and harvest time that affect the garlic biosynthesis of phenolic and its organosulfur compounds (Lu et al. 2011; Montano et al. 2011). The TPC present in garlic extracts were significantly higher than the microencapsulated powders. These results suggest some loss of

**Table 4** Total phenolic content (TPC) (mg GAE  $g^{-1}$  d.b.) and ABTS capacity ( $\mu\text{mol TE } g^{-1}$  d.b.) of garlic extract (GE) at pH 3.6 and 5.5 and WPI/CH and GA/CH microparticles obtained by complex coacervation followed by freeze-drying process

Antioxidative properties	Samples			
	GE-3.6	GE-5.5	WPI/CH	GA/CH
TPC (mg GAE $g^{-1}$ d.b.)	17.24 $\pm$ 0.06 <sup>a</sup>	15.33 $\pm$ 0.21 <sup>b</sup>	12.92 $\pm$ 0.28 <sup>d</sup>	13.49 $\pm$ 0.02 <sup>c</sup>
ABTS ( $\mu\text{mol TE } g^{-1}$ d.b.)	8.52 $\pm$ 0.91 <sup>a</sup>	9.75 $\pm$ 0.89 <sup>a</sup>	7.69 $\pm$ 0.21 <sup>b</sup>	7.79 $\pm$ 0.17 <sup>b</sup>
TPC retention (%)	–	–	78.26	89.34

Different letters in the same column indicate values that are significantly different ( $p < 0.05$ ) based on Tukey's multiple comparison test

unprotected garlic phenolic compounds in the complex coacervation process. In the freeze-drying process, the grinding of the freeze-dried product may lead to degradation of garlic bioactive compounds due to oxidation reaction (Kuck and Noreña 2016). The WPI/CH and GA/CH microparticles revealed efficiently in the entrapment of garlic phenolic compounds with retention of 84% and 78%, respectively. The production of WPI/CH microparticles by freeze-drying revealed more efficiently in the phenolic compounds retention than by spray drying reported by Tavares and Noreña (2019) with retention of 61.40%. The high temperatures in the spray drying process mainly caused degradation of volatile compounds present in garlic, degradation, and polymerization of unencapsulated phenolic compounds. The higher concentrations of phenolic compounds give a higher possibility for their application in food preparation and in food industry.

The antioxidant potential of the garlic extracts (pH 3.6 and 5.5) and microparticles powders was determined on the basis of the scavenging activity of the stable free radicals ABTS (Table 4). This assay compares the capacity of the samples to quench the ABTS<sup>+</sup> radical cation, and the results are expressed as Trolox reference antioxidant. The pH had no influence on antioxidant activity of the garlic extract. The results of garlic antioxidant activity were lower than reported by Tavares and Noreña (2019), mainly due to the difference in the garlic type, origin, and cultivation conditions. The WPI/CH and GA/CH microparticles showed high antioxidant potential, but the antioxidant activity of garlic extracts was higher, indicating that not all garlic bioactive compounds were well encapsulated. These results are in accordance with the verified in the assay to determine the TPC since there exists strong correlation between total phenolic content and antioxidant activity present in garlic extract (Lanzotti 2006). Studies have been demonstrated that CH and WPI have antioxidant activity (Chang et al. 2018; de Castro et al. 2017).

## Conclusion

In the present study, two anionic biopolymers (Arabic gum and WPI) were used to find the most suitable wall materials to interact electrostatically with cationic chitosan (CH) to encapsulate garlic extract. The encapsulation by complex coacervation followed by freeze-drying allowed to protect heat-sensitive compounds present in garlic extract. The freeze-dried powders showed disordered domains (amorphous structure), irregular shape and size, and cracking and craters evidences on the structure, suggesting that the garlic bioactive compounds were protected and incorporated into biopolymer matrices. The nitrogen adsorption revealed powerful technique to determine the small pores diameters of microparticles, unlike SEM imaging where small pores cannot be detected due to its limited resolution. FTIR study of microparticles

revealed no chemical cross-linking reaction between garlic compounds and wall materials complexes, indicating that the garlic compounds were incorporated into complex wall materials by physical interaction. The anionic GA was better than WPI for coacervation with cationic chitosan in terms of less hygroscopicity, smaller particle size and higher retention of garlic phenolic compounds, resulting in microparticles with better chemical, physical, and structural properties. However, both microparticles revealed promising potential to be used as ingredients in the elaboration of functional foods (such as soup and bakery products), due to its high content of phenolic compounds and antioxidant activity.

**Acknowledgments** We thank the Primex (Siglufjörður, Iceland) and Arla Foods Ingredients for donating chitosan and whey proteins isolates, respectively.

**Funding Information** The authors received financial support provided by CNPq and FAPERGS. Loleny Tavares received scholarship funding from the CAPES/CNPq-Programa Estudantes-Convênio de Pós-Graduação (PEC-PG).

## References

- Alishahi, A., & Aider, M. (2012). Applications of chitosan in the seafood industry and aquaculture: a review. *Food and Bioprocess Technology*, 5(3), 817–830.
- Almeida, C. M., Magalhães, J. M., Souza, H. K., & Gonçalves, M. P. (2018). The role of choline chloride-based deep eutectic solvent and curcumin on chitosan films properties. *Food Hydrocolloids*, 81, 456–466.
- Amagase, H., Petesch, B. L., Matsuura, H., Kasuga, S., & Itakura, Y. (2001). Intake of garlic and its bioactive components. *The Journal of Nutrition*, 131(3), 955S–962S.
- Anderson, R. B. (1946). Modifications of the Brunauer, Emmett and Teller equation<sup>1</sup>. *Journal of the American Chemical Society*, 68(4), 686–691.
- AOAC. (1990). *Official methods of analysis of the association of official analytical chemists*. Washington, DC: AOAC.
- Arthur, E., Tuller, M., Moldrup, P., Greve, M. H., Knadel, M., & de Jonge, L. W. (2018). Applicability of the Guggenheim–Anderson–Boer water vapour sorption model for estimation of soil specific surface area. *European Journal of Soil Science*, 69(2), 245–255.
- Azizi, M., Kierulf, A., Lee, M. C., & Abbaspourrad, A. (2018). Improvement of physicochemical properties of encapsulated echium oil using nanostructured lipid carriers. *Food Chemistry*, 246, 448–456.
- Balasubramani, P., Palaniswamy, P., Visvanathan, R., Thirupathi, V., Subbarayan, A., & Maran, J. P. (2015). Microencapsulation of garlic oleoresin using maltodextrin as wall material by spray drying technology. *International Journal of Biological Macromolecules*, 72, 210–217.
- Barrett, E. P., Joyner, L. G., & Halenda, P. (1951). The determination of pore volume and area distributions in porous substances. I. Computations from nitrogen isotherms. *Journal of the American Chemical Society*, 73(1), 373–380.
- Bastos, D. S., Barreto, B. N., Souza, H. K., Bastos, M., Rocha-Leão, M. H. M., Andrade, C. T., et al. (2010). Characterization of a chitosan sample extracted from Brazilian shrimps and its application to obtain



- insoluble complexes with a commercial whey protein isolate. *Food Hydrocolloids*, 24(8), 709–718.
- Bormann, D., Pierucci, A. P. T. R., Leite, S. G. F., & da Rocha Leão, M. H. M. (2013). Microencapsulation of passion fruit (*Passiflora*) juice with n-octenylsuccinate-derivatized starch using spray-drying. *Food and Bioprocess Processing*, 91(1), 23–27.
- Brunauer, S., Emmett, P. H., & Teller, E. (1938). Adsorption of gases in multimolecular layers. *Journal of the American Chemical Society*, 60(2), 309–319.
- Brunauer, S., Deming, L. S., Deming, W. E., & Teller, E. (1940). On a theory of the van der Waals adsorption of gases. *Journal of the American Chemical Society*, 62(7), 1723–1732.
- Burgess, D. (1990). Practical analysis of complex coacervate systems. *Journal of Colloid and Interface Science*, 140(1), 227–238.
- Butstraen, C., & Salaün, F. (2014). Preparation of microcapsules by complex coacervation of gum Arabic and chitosan. *Carbohydrate Polymers*, 99, 608–616.
- Cabuk, M., Yavuz, M., & Unal, H. I. (2016). Electrokinetic, electrorheological and viscoelastic properties of Polythiophene-graft-Chitosan copolymer particles. *Colloids and Surfaces A: Physicochemical and Engineering Aspects*, 510, 231–238.
- Cai, Y., & Corke, H. (2000). Production and properties of spray-dried amaranthus betacyanin pigments. *Journal of Food Science*, 65(7), 1248–1252.
- Cano-Chauca, M., Stringheta, P., Ramos, A., & Cal-Vidal, J. (2005). Effect of the carriers on the microstructure of mango powder obtained by spray drying and its functional characterization. *Innovative Food Science & Emerging Technologies*, 6(4), 420–428.
- Chang, S.-H., Wu, C.-H., & Tsai, G.-J. (2018). Effects of chitosan molecular weight on its antioxidant and antimutagenic properties. *Carbohydrate Polymers*, 181, 1026–1032.
- Chen, C., Chi, Y.-J., & Xu, W. (2012). Comparisons on the functional properties and antioxidant activity of spray-dried and freeze-dried egg white protein hydrolysate. *Food and Bioprocess Technology*, 5(6), 2342–2352.
- Chen, C., Liu, C.-H., Cai, J., Zhang, W., Qi, W.-L., Wang, Z., et al. (2018). Broad-spectrum antimicrobial activity, chemical composition and mechanism of action of garlic (*Allium sativum*) extracts. *Food Control*, 86, 117–125.
- Choi, Y.-R., & Chang, Y. H. (2018). Microencapsulation of gallic acid through the complex of whey protein concentrate-pectic polysaccharide extracted from *Ulmus davidiana*. *Food Hydrocolloids*, 85, 222–228.
- da Costa, J. M. G., Silva, E. K., Hijo, A. A. C. T., Azevedo, V. M., Malta, M. R., Alves, J. G. L. F., et al. (2015). Microencapsulation of Swiss cheese bioaroma by spray-drying: process optimization and characterization of particles. *Powder Technology*, 274, 296–304.
- Damodaran, S., & Parkin, K. L. (2017). *Fennema's food chemistry*. Boca Raton: CRC Press.
- de Castro, R. J. S., Domingues, M. A. F., Ohara, A., Okuro, P. K., dos Santos, J. G., Brexó, R. P., et al. (2017). Whey protein as a key component in food systems: physicochemical properties, production technologies and applications. *Food Structure*, 14, 17–29.
- de Souza, H. K., Bai, G., & do Pilar Gonçalves, M., & Bastos, M. (2009). Whey protein isolate–chitosan interactions: a calorimetric and spectroscopy study. *Thermochimica Acta*, 495(1), 108–114.
- Eratte, D., Wang, B., Dowling, K., Barrow, C. J., & Adhikari, B. P. (2014). Complex coacervation with whey protein isolate and gum arabic for the microencapsulation of omega-3 rich tuna oil. *Food & Function*, 5(11), 2743–2750.
- Eratte, D., Dowling, K., Barrow, C. J., & Adhikari, B. (2018). Recent advances in the microencapsulation of omega-3 oil and probiotic bacteria through complex coacervation: a review. *Trends in Food Science & Technology*, 71, 121–131.
- Espinosa-Andrews, H., Sandoval-Castilla, O., Vázquez-Torres, H., Vernon-Carter, E. J., & Lobato-Calleros, C. (2010). Determination of the gum Arabic–chitosan interactions by Fourier transform infrared spectroscopy and characterization of the microstructure and rheological features of their coacervates. *Carbohydrate Polymers*, 79(3), 541–546.
- Ezhilarasi, P., Karthik, P., Chhanwal, N., & Anandharamakrishnan, C. (2013). Nanoencapsulation techniques for food bioactive components: a review. *Food and Bioprocess Technology*, 6, 628–647.
- Fernandes, R. V. d. B., Borges, S. V., Botrel, D. A., & Oliveira, C. R. d. (2014). Physical and chemical properties of encapsulated rosemary essential oil by spray drying using whey protein–inulin blends as carriers. *International Journal of Food Science & Technology*, 49(6), 1522–1529.
- Fernandes, R. V. d. B., Borges, S. V., Silva, E. K., da Silva, Y. F., de Souza, H. J. B., do Carmo, E. L., et al. (2016). Study of ultrasound-assisted emulsions on microencapsulation of ginger essential oil by spray drying. *Industrial Crops and Products*, 94, 413–423.
- Fu, J., Xu, Q., Chen, J., Chen, Z., Huang, X., & Tang, X. (2010). Controlled fabrication of uniform hollow core porous shell carbon spheres by the pyrolysis of core/shell polystyrene/cross-linked polyphosphazene composites. *Chemical Communications*, 46(35), 6563–6565.
- Gámiz-González, M., Correia, D. M., Lanceros-Mendez, S., Sencadas, V., Ribelles, J. G., & Vidaurre, A. (2017). Kinetic study of thermal degradation of chitosan as a function of deacetylation degree. *Carbohydrate Polymers*, 167, 52–58.
- González-Martínez, D., Carrillo-Navas, H., Barrera-Díaz, C., Martínez-Vargas, S., Álvarez-Ramírez, J., & Pérez-Alonso, C. (2017). Characterization of a novel complex coacervate based on whey protein isolate-tamarind seed mucilage. *Food Hydrocolloids*, 72, 115–126.
- Hosseini, S. F., Zandi, M., Rezaei, M., & Farahmandghavi, F. (2013). Two-step method for encapsulation of oregano essential oil in chitosan nanoparticles: preparation, characterization and in vitro release study. *Carbohydrate Polymers*, 95(1), 50–56.
- Huang, G.-Q., Sun, Y.-T., Xiao, J.-X., & Yang, J. (2012). Complex coacervation of soybean protein isolate and chitosan. *Food Chemistry*, 135(2), 534–539.
- Ilić, J. D., Nikolovski, B. G., Petrović, L. B., Kojić, P. S., Lončarević, I. S., & Petrović, J. S. (2017). The garlic (*A. sativum* L.) extracts food grade W1/O/W2 emulsions prepared by homogenization and stirred cell membrane emulsification. *Journal of Food Engineering*, 205, 1–11.
- Kang, Y.-R., Lee, Y.-K., Kim, Y. J., & Chang, Y. H. (2019). Characterization and storage stability of chlorophylls microencapsulated in different combination of gum Arabic and maltodextrin. *Food Chemistry*, 272, 337–346.
- Khem, S., Small, D. M., & May, B. K. (2016). The behaviour of whey protein isolate in protecting *Lactobacillus plantarum*. *Food Chemistry*, 190, 717–723.
- Kinalski, T., & Noreña, C. P. Z. (2014). Effect of blanching treatments on antioxidant activity and thiosulfinate degradation of garlic (*Allium sativum* L.). *Food and Bioprocess Technology*, 7, 2152–2157.
- Kinalski, T., & Noreña, C. P. Z. (2019). Effect of spray drying encapsulation of garlic extract on inulin and thiosulfinate contents. *Food and Bioprocess Technology*, 13, 2438–2447.
- Koç, B., Yilmazer, M. S., Balkır, P., & Ertekin, F. K. (2010). Moisture sorption isotherms and storage stability of spray-dried yogurt powder. *Drying Technology*, 28(6), 816–822.
- Krishnamachari, Y., Madan, P., & Lin, S. (2007). Development of pH- and time-dependent oral microparticles to optimize budesonide delivery to ileum and colon. *International Journal of Pharmaceutics*, 338(1–2), 238–247.
- Kuck, L. S., & Noreña, C. P. Z. (2016). Microencapsulation of grape (*Vitis labrusca* var. Bordo) skin phenolic extract using gum Arabic, polydextrose, and partially hydrolyzed guar gum as encapsulating agents. *Food Chemistry*, 194, 569–576.



- Lago, C. C., & Noreña, C. P. Z. (2015). Thermodynamic analysis of sorption isotherms of dehydrated yacon (Smallanthus sonchifolius) bagasse. *Food Bioscience*, 12, 26–33.
- Lam, B., Déon, S., Morin-Crini, N., Crini, G., & Fievet, P. (2018). Polymer-enhanced ultrafiltration for heavy metal removal: influence of chitosan and carboxymethyl cellulose on filtration performances. *Journal of Cleaner Production*, 171, 927–933.
- Lanzotti, V. (2006). The analysis of onion and garlic. *Journal of Chromatography A*, 1112(1–2), 3–22.
- Lewicki, P. P. (1997). The applicability of the GAB model to food water sorption isotherms. *International Journal of Food Science & Technology*, 32(6), 553–557.
- Liu, X., Xiong, J., & Liang, L. (2015). Investigation of pore structure and fractal characteristics of organic-rich Yanchang formation shale in central China by nitrogen adsorption/desorption analysis. *Journal of Natural Gas Science and Engineering*, 22, 62–72.
- Lomauro, C., Bakshi, A., & Labuza, T. P. (1985). Evaluation of food moisture sorption isotherm equations part II: milk, coffee, tea, nuts, oilseeds, spices and starchy foods. *LWT- Food Science and Technology*, 18(2), 118–124.
- Lu, X., Ross, C. F., Powers, J. R., Aston, D. E., & Rasco, B. A. (2011). Determination of total phenolic content and antioxidant activity of garlic (*Allium sativum*) and elephant garlic (*Allium ampeloprasum*) by attenuated total reflectance–Fourier transformed infrared spectroscopy. *Journal of Agricultural and Food Chemistry*, 59(10), 5215–5221.
- Martins, N., Petropoulos, S., & Ferreira, I. C. F. R. (2016). Chemical composition and bioactive compounds of garlic (*Allium sativum* L.) as affected by pre- and post-harvest conditions: A review. *Food Chemistry*, 211, 41–50.
- Meng, F., Wang, S., Liu, H., Xu, X., & Ma, H. (2017). Microencapsulation of oxalic acid (OA) via coacervation induced by polydimethylsiloxane (PDMS) for the sustained release performance. *Materials & Design*, 116, 31–41.
- Montano, A., Beato, V. M., Mansilla, F., & Orgaz, F. (2011). Effect of genetic characteristics and environmental factors on organosulfur compounds in garlic (*Allium sativum* L.) grown in Andalusia, Spain. *Journal of Agricultural and Food Chemistry*, 59(4), 1301–1307.
- Niu, F., Niu, D., Zhang, H., Chang, C., Gu, L., Su, Y., et al. (2016). Ovalbumin/gum arabic-stabilized emulsion: rheology, emulsion characteristics, and Raman spectroscopic study. *Food Hydrocolloids*, 52, 607–614.
- Noreña, C. P. Z., Bayarri, S., & Costell, E. J. F. B. (2015). Effects of xanthan gum additions on the viscoelasticity, structure and storage stability characteristics of prebiotic custard desserts. *Food Biophysics*, 10(2), 116–128.
- Nuutila, A. M., Puupponen-Pimiä, R., Aarni, M., & Oksman-Caldentey, K.-M. (2003). Comparison of antioxidant activities of onion and garlic extracts by inhibition of lipid peroxidation and radical scavenging activity. *Food Chemistry*, 81(4), 485–493.
- Peng, X., Li, R., Zou, R., Chen, J., Zhang, Q., Cui, P., et al. (2014). Allicin inhibits microbial growth and oxidative browning of fresh-cut lettuce (*Lactuca sativa*) during refrigerated storage. *Food and Bioprocess Technology*, 7(6), 1597–1605.
- Peniche, C., Argüelles-Monal, W., Peniche, H., & Acosta, N. (2003). Chitosan: an attractive biocompatible polymer for microencapsulation. *Macromolecular Bioscience*, 3(10), 511–520.
- Piletti, R., Zanetti, M., Jung, G., de Mello, J. M. M., Dalcanton, F., Soares, C., Riella, H. G., & Fiori, M. A. (2019). Microencapsulation of garlic oil by  $\beta$ -cyclodextrin as a thermal protection method for antibacterial action. *Materials Science and Engineering: C*, 94, 139–149.
- Pinilla, C. M. B., & Brandelli, A. (2016). Antimicrobial activity of nanoliposomes co-encapsulating nisin and garlic extract against Gram-positive and Gram-negative bacteria in milk. *Innovative Food Science & Emerging Technologies*, 36, 287–293.
- Pinilla, C. M. B., Noreña, C. P. Z., & Brandelli, A. (2017). Development and characterization of phosphatidylcholine nanovesicles, containing garlic extract, with antilisterial activity in milk. *Food Chemistry*, 220, 470–476.
- Premi, M., & Sharma, H. (2017). Effect of different combinations of maltodextrin, gum arabic and whey protein concentrate on the encapsulation behavior and oxidative stability of spray dried drumstick (*Moringa oleifera*) oil. *International Journal of Biological Macromolecules*, 105, 1232–1240.
- Quispe-Condori, S., Saldaña, M. D., & Temelli, F. (2011). Microencapsulation of flax oil with zein using spray and freeze drying. *LWT- Food Science and Technology*, 44(9), 1880–1887.
- Re, R., Pellegrini, N., Proteggente, A., Pannala, A., Yang, M., & Rice-Evans, C. (1999). Antioxidant activity applying an improved ABTS radical cation decolorization assay. *Free Radical Biology and Medicine*, 26(9), 1231–1237.
- Robert, P., Gorena, T., Romero, N., Sepulveda, E., Chavez, J., & Saenz, C. (2010). Encapsulation of polyphenols and anthocyanins from pomegranate (*Punica granatum*) by spray drying. *International Journal of Food Science & Technology*, 45(7), 1386–1394.
- Rocha-Selmi, G. A., Theodoro, A. C., Thomazini, M., Bolini, H. M., & Favaro-Trindade, C. S. (2013). Double emulsion stage prior to complex coacervation process for microencapsulation of sweetener sucralose. *Journal of Food Engineering*, 119(1), 28–32.
- Santhosha, S. G., Jamuna, P., & Prabhavathi, S. N. (2013). Bioactive components of garlic and their physiological role in health maintenance: a review. *Food Bioscience*, 3, 59–74.
- Santos, M. G., Bozza, F. T., Thomazini, M., & Favaro-Trindade, C. S. (2015). Microencapsulation of xylitol by double emulsion followed by complex coacervation. *Food Chemistry*, 171, 32–39.
- Shi, Y., Li, C., Zhang, L., Huang, T., Ma, D., Tu, Z.-c., et al. (2017). Characterization and emulsifying properties of octenyl succinate anhydride modified Acacia seyal gum (gum arabic). *Food Hydrocolloids*, 65, 10–16.
- Sing, K. S. (1985). Reporting physisorption data for gas/solid systems with special reference to the determination of surface area and porosity (Recommendations 1984). *Pure and Applied Chemistry*, 57(4), 603–619.
- Singleton, V., & Rossi, J. A. (1965). Colorimetry of total phenolics with phosphomolybdic-phosphotungstic acid reagents. *American Journal of Enology and Viticulture*, 16(3), 144–158.
- Spiess, W., & Wolf, W. (1983). Results of the COST 90 project on water activity. In R. Jowitt (Ed.), *Physical properties of foods*. London: Applied Science Publishers.
- Szulińska, M., Kręgielska-Narożna, M., Świątek, J., Styś, P., Kuźnar-Kamińska, B., Jakubowski, H., Walkowiak, J., & Bogdański, P. (2018). Garlic extract favorably modifies markers of endothelial function in obese patients—randomized double blind placebo-controlled nutritional intervention. *Biomedicine & Pharmacotherapy*, 102, 792–797.
- Tan, C., Xie, J., Zhang, X., Cai, J., & Xia, S. (2016). Polysaccharide-based nanoparticles by chitosan and gum arabic polyelectrolyte complexation as carriers for curcumin. *Food Hydrocolloids*, 57, 236–245.
- Tavares, L., & Noreña, C. P. Z. (2019). Encapsulation of garlic extract using complex coacervation with whey protein isolate and chitosan as wall materials followed by spray drying. *Food Hydrocolloids*, 89, 360–369.
- Timilsena, Y. P., Akanbi, T. O., Khalid, N., Adhikari, B., & Barrow, C. J. (2018). Complex coacervation: Principles, mechanisms and applications in microencapsulation. *International Journal of Biological Macromolecules*, 121, 1276–1286.
- Tomšik, A., Šarić, L., Bertoni, S., Protti, M., Albertini, B., Mercolini, L., et al. (2018). Encapsulations of wild garlic (*Allium ursinum* L.)

- extract using spray congealing technology. *Food Research International*, 119, 941–950.
- Tonon, R. V., Brabet, C., & Hubinger, M. D. (2008). Influence of process conditions on the physicochemical properties of açai (*Euterpe oleracea* Mart.) powder produced by spray drying. *Journal of Food Engineering*, 88(3), 411–418.
- Tonon, R. V., Brabet, C., Pallet, D., Brat, P., & Hubinger, M. D. (2009). Physicochemical and morphological characterisation of açai (*Euterpe oleracea* Mart.) powder produced with different carrier agents. *International Journal of Food Science & Technology*, 44(10), 1950–1958.
- Włodarczyk-Stasiak, M., Mazurek, A., Pankiewicz, U., Sujka, M., & Jamroz, J. (2014). Porosity of starch–proteins extrudates determined from nitrogen adsorption data. *Food Hydrocolloids*, 36, 308–315.
- Wolf, W., Spiess, W., & Jung, G. (1985). Standardization of isotherm measurements (COST-project 90 and 90 bis). In D. Simatos & J. L. Multon (Eds.), *Properties of water in foods* (pp. 661–679). Dordrecht: Springer.
- Xu, D., Aihemaiti, Z., Cao, Y., Teng, C., & Li, X. (2016). Physicochemical stability, microrheological properties and microstructure of lutein emulsions stabilized by multilayer membranes consisting of whey protein isolate, flaxseed gum and chitosan. *Food Chemistry*, 202, 156–164.
- Young, J. F. (1967). Humidity control in the laboratory using salt solutions—a review. *Journal of Applied Chemistry*, 17(9), 241–245.

**Publisher's Note** Springer Nature remains neutral with regard to jurisdictional claims in published maps and institutional affiliations.